

Synthesis, Structures, and Properties of the Phosphonium-1-indenylide (PHIN) Ligands 1-C₉H₆PPh₃, 1-C₉H₆PMePh₂, and 1-C₉H₆PMe₂Ph and of the Corresponding Ruthenium(II) Complexes [Ru(η^5 -C₅H₅)(η^5 -PHIN)]PF₆

Kevin G. Fowler, Shalyn L. Littlefield, and Michael C. Baird*

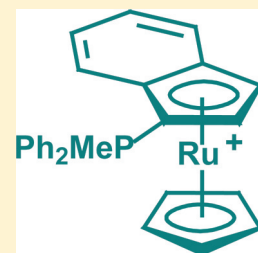
Department of Chemistry, Queen's University, Kingston, Ontario K7L 3N6, Canada

Peter H. M. Budzelaar*

Department of Chemistry, University of Manitoba, Winnipeg, Manitoba R3T 2N2, Canada

S Supporting Information

ABSTRACT: Syntheses of the phosphonium-1-indenylide (PHIN) ligands triphenylphosphonium-1-indenylide (1-C₉H₆PPh₃, **I**), methyl-diphenylphosphonium-1-indenylide (1-C₉H₆PMePh₂, **II**), and dimethylphenylphosphonium-1-indenylide (1-C₉H₆PMe₂Ph, **III**) are reported, as are syntheses of the corresponding planar chiral ruthenium(II) complexes [Ru(η^5 -C₅H₅)(η^5 -1-C₉H₆PPh₃)]PF₆ (**IV**), [Ru(η^5 -C₅H₅)(η^5 -1-C₉H₆PMePh₂)]PF₆ (**V**), and [Ru(η^5 -C₅H₅)(η^5 -1-C₉H₆PMe₂Ph)]PF₆ (**VI**). The ruthenium complexes have been characterized by ¹H, ¹³C, and ³¹P NMR spectroscopy, by X-ray crystallography, and by extensive DFT calculations, which produce optimized geometries consistent with the crystallographic data. The PHIN–Ru bond strengths are calculated to be ~20 kcal/mol greater than the corresponding benzene–Ru bond strength of [Ru(η^5 -C₅H₅)(η^6 -C₆H₆)]⁺ and are compatible with the observed configurational stability of the complexes. That interconversion of enantiomers via interfacial exchange of the η^5 -bound ligands does not occur is demonstrated by the observation of diastereotopic phenyl groups in the ¹H NMR spectrum of **V** and of diastereotopic methyl groups in the ¹H NMR spectrum of **VI**.



The compound triphenylphosphonium cyclopentadienylide, C₅H₄PPh₃ (Figure 1), was first reported in 1956 by

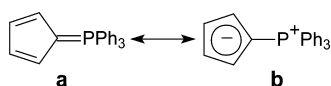


Figure 1. Resonance structures of C₅H₄PPh₃.

Ramirez and Levy,¹ who found inter alia that this ylide is unusually inert. Unlike normal ylides, for instance, it does not react with ketones. This unusual stability was attributed to the electron delocalization implied by the zwitterionic resonance structure **b**, consistent with the relatively high dipole moment of 7.0 D.^{1c}

Further evidence for the relevance of **b** was found crystallographically in the P–C₅H₄ bond length and the C–C distances in the five-membered ring^{1g} and in the ¹³C NMR spectrum, which exhibited an unusually high field chemical shift for the ylide carbon and a P–C(ylide) coupling constant typical of an aliphatic carbon–P bond.^{1h} Phosphonium cyclopentadienylides of this type are thus isoelectronic with neutral arene and anionic cyclopentadienyl ligands and are expected to exhibit an extensive coordination chemistry.²

That said, however, as we noted in 2007,^{3a} the coordination chemistry of this class of very interesting ligands has received

little systematic attention, in spite of its clear potential. We therefore initiated an investigation of transition-metal coordination complexes of phosphonium cyclopentadienylides and reported the synthesis and reactivity of the group 6 compounds M(η^5 -C₅H₄PMePh₂)(CO)₃ (M = Cr, Mo, W), containing C₅H₄PMePh₂, methyl-diphenylphosphonium cyclopentadienylide.³ This ligand was chosen over the Ramirez ylide because much less had been done with it and the methyl group provided a useful NMR “handle”. We found, inter alia, that the donor properties of C₅H₄PMePh₂ fall between those of benzene and the cyclopentadienyl (η^5 -C₅H₅) ligand,³ consistent with the presence of a partial negative charge on the five-membered ring and suggesting that there would be interesting comparisons and contrasts to be made with the coordination chemistry of similar arene and cyclopentadienyl complexes.

We also investigated the electronic structures of C₅H₄PMePh₂ and Cr(η^5 -C₅H₄PMePh₂)(CO)₃ using ab initio methodologies, finding that the near-degenerate HOMO and HOMO-1 orbitals of the free ylide exhibit symmetries very similar to those of the corresponding, doubly degenerate HOMO of the cyclopentadienyl anion (E₁ symmetry). We also found that a lower energy, almost fully symmetric orbital corresponds to the fully symmetric bonding A₁ MO of the

Received: June 25, 2011

Published: October 24, 2011

cyclopentadienyl anion. In none of these three orbitals did there appear to be significant π involvement with an orbital on the phosphorus atom, consistent with the low P–C bond order implicit in zwitterionic structure **b**. The primary ylide–metal interactions in $\text{Cr}(\eta^5\text{-C}_5\text{H}_4\text{PMePh}_2)(\text{CO})_3$ were found to involve donation of the HOMO and HOMO-1 orbitals into the d_{xz} and d_{yz} orbitals of the chromium, respectively, while the calculated ylide– $\text{Cr}(\text{CO})_3$ bond dissociation energy was about 30% higher than the analogous ring–metal bond dissociation energy calculated for $(\eta^6\text{-C}_6\text{H}_6)\text{Cr}(\text{CO})_3$.

In order to extend the chemistry of this class of ligand, we subsequently began an investigation of the analogous phosphonium-1-indenylide (PHIN) ligands, beginning with methyl-diphenylphosphonium-1-indenylide, $1\text{-C}_9\text{H}_6\text{PMePh}_2$ (Figure 2).⁴

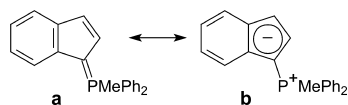


Figure 2. Resonance structures of $1\text{-C}_9\text{H}_6\text{PMePh}_2$.

The first such ligand, triphenylphosphonium-1-indenylide ($1\text{-C}_9\text{H}_6\text{PPh}_3$), was reported in the 1960s, although it was not characterized by NMR spectroscopy or crystallography.⁵ Two much better characterized analogues, $1\text{-C}_9\text{H}_6\text{P}(\text{CH}_2\text{Ph})\text{Ph}_2$ and $1\text{-C}_9\text{H}_6\text{P}(\text{CH}_2\text{C}_6\text{F}_5)\text{Ph}_2$, were subsequently reported in 2004,⁶ but the coordination chemistry of these three aromatic ligands has not been investigated and, indeed, to our knowledge no other indenyl-derived phosphorus ylides have been reported. Adding to our interest, ligands of the type $1\text{-C}_9\text{H}_6\text{PR}_3$ are planar prochiral, with the result that their coordination compounds exhibit planar chirality (Figure 3). Thus, as an

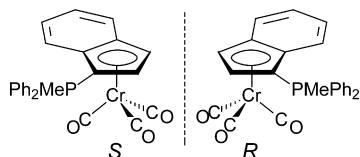


Figure 3. Enantiomers of the chiral complex $\text{Cr}(\eta^5\text{-}1\text{-C}_9\text{H}_6\text{PMePh}_2)(\text{CO})_3$.

example, we reported the synthesis and characterization, including crystallography, of the planar chiral chromium compound $\text{Cr}(\eta^5\text{-}1\text{-C}_9\text{H}_6\text{PMePh}_2)(\text{CO})_3$.⁴ On the basis of the IR spectrum in the carbonyl region, the indenylidene ligand was found to exhibit donor properties very similar to those of its cyclopentadienylidene analogue.⁴

We have now extended the list of well-characterized phosphonium-1-indenylide (PHIN) ligands and report herein the synthesis and full characterization of the aforementioned triphenylphosphonium-1-indenylide ($1\text{-C}_9\text{H}_6\text{PPh}_3$, **I**), a new procedure for the synthesis of the known $1\text{-C}_9\text{H}_6\text{PMePh}_2$ (**II**), and the synthesis and characterization of the new ligand dimethylphenylphosphonium-1-indenylide ($1\text{-C}_9\text{H}_6\text{PMe}_2\text{Ph}$, **III**). Furthermore, with a view to extending and investigating the coordination chemistry of PHIN ligands to complexes of metals in oxidation states higher than 0, we also describe the synthesis, structures, and mode of bonding of the ruthenium-(**II**) complexes $[\text{Ru}(\eta^5\text{-C}_5\text{H}_5)(\eta^5\text{-}1\text{-C}_9\text{H}_6\text{PPh}_3)]\text{PF}_6$ (**IV**), $[\text{Ru}(\eta^5\text{-C}_5\text{H}_5)(\eta^5\text{-}1\text{-C}_9\text{H}_6\text{PMePh}_2)]\text{PF}_6$ (**V**), and $[\text{Ru}(\eta^5\text{-C}_5\text{H}_5)(\eta^5\text{-}1\text{-C}_9\text{H}_6\text{PMe}_2\text{Ph})]\text{PF}_6$ (**VI**) (Figure 4).

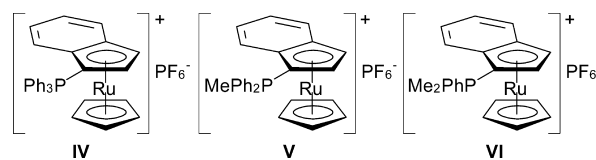


Figure 4. Ruthenium complexes studied.

RESULTS AND DISCUSSION

Ligand Syntheses and NMR Characterization. We previously prepared **II** via a procedure which involved the synthesis of $\text{P}(1\text{-indenyl})\text{Ph}_2$ via reaction of lithium indenylide with chlorodiphenylphosphine, followed by methylation and deprotonation steps as shown in Figure 5.

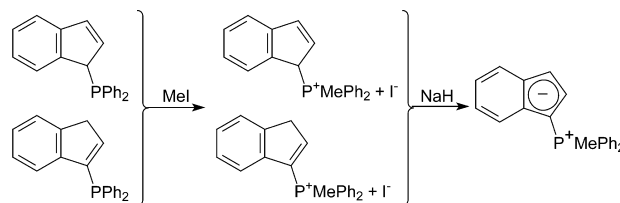


Figure 5. Previously utilized procedure for the synthesis of **II**.

This procedure is not of general utility, however, as few dialkyl- or diarylmonochlorophosphines are readily available. We have therefore developed the more general route shown in Figure 6, which also shows the ring atom numbering scheme

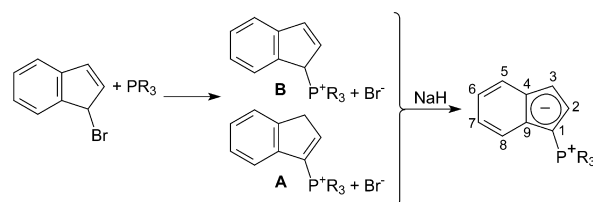


Figure 6. General procedure for the synthesis of phosphonium-1-indenylides ($R = \text{methyl, phenyl}$) and numbering scheme for the ring sites.

used below in discussions of the NMR spectra and the crystal structures of the PHIN ligands **I–III** and their coordination complexes **IV–VI**.

Thus, 1-bromoindene, prepared via the bromination of 1-trimethylsilylindene by dioxane dibromide,⁷ was reacted with the tertiary phosphines PPh_3 , PMePh_2 , and PMe_2Ph as shown in Figure 6 to form the corresponding phosphonium salts as mixtures of regioisomers **A** and **B** as indicated. The product mixtures were characterized by ^1H and ^{31}P NMR spectroscopy, and as an example, the ^1H NMR spectrum of $(1\text{-C}_9\text{H}_7\text{PMe}_2\text{Ph})\text{Br}$ is shown in Figure 7.

As can be seen, the olefinic and aromatic resonances of the pairs of regioisomers overlap considerably in the region δ 6.3–8.3, and assignments of these resonances were not attempted. In contrast, the methylene resonance of isomer **A** and the methyl resonances of both **A** and **B** are readily identified. Interestingly, since isomer **B** contains a chiral center at C(1), the two methyl groups are diastereotopic and exhibit distinct ^1H resonances as shown.

The ^1H NMR spectra of $(1\text{-C}_9\text{H}_7\text{PPh}_3)\text{Br}$ and $(1\text{-C}_9\text{H}_7\text{PMePh}_2)\text{Br}$ (Figures S1 and S2, respectively, in the

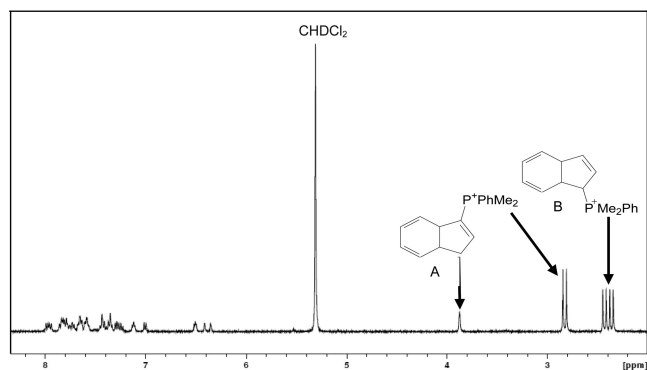


Figure 7. ^1H NMR spectrum of $(1\text{-C}_9\text{H}_7\text{PMe}_2\text{Ph})\text{Br}$.

Supporting Information) were also complex in the olefinic and aromatic regions, but the chemical shifts of the various proton environments are clearly similar to the corresponding chemical shifts of $(1\text{-C}_9\text{H}_7\text{PMe}_2\text{Ph})\text{Br}$. The ^{31}P NMR spectra of each of the three phosphonium salts exhibited two distinct ^{31}P resonances (see the Experimental Section), and thus the ratios of regioisomers were readily obtained. The relative amounts were found to vary seemingly randomly from batch to batch, but we have not attempted to ascertain the reason(s).

The free PHIN ligands $1\text{-C}_9\text{H}_6\text{PPh}_3$ (I), $1\text{-C}_9\text{H}_6\text{PMePh}_2$ (II), and $1\text{-C}_9\text{H}_6\text{PMe}_2\text{Ph}$ (III) were readily synthesized in good yields from their respective phosphonium salts by deprotonation using an excess of NaH in THF. Ylide II has been previously characterized by NMR spectroscopy and X-ray crystallography,⁴ and ylides I and III have now also been characterized by crystallography (see below) and by NMR spectroscopy utilizing COSY, NOESY, HSQC, and HMBC experiments. The ^1H NMR spectrum of III is shown in Figure 8, NMR spectroscopic data (^1H , ^{13}C) for all three

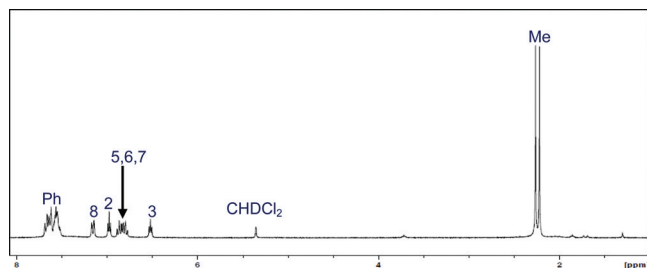
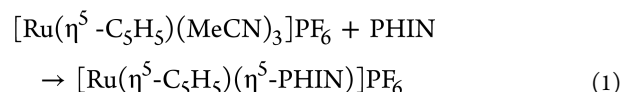


Figure 8. ^1H NMR spectrum of $1\text{-C}_9\text{H}_6\text{PMe}_2\text{Ph}$ (III).

ylides are given in Tables 1–3, and ^1H NMR spectra of I and II are shown in Figures S3 and S4, respectively, of the Supporting Information.

As can be seen from Figure 8, the methyl resonance of III is observed as the expected doublet, with $J_{\text{P-H}} = 13.2$ Hz, and the resonances of the 1-indenyl group, H(2)–H(8), are upfield and well separated from those of the phenyl group. Similar upfield shifts are observed for I and II (Tables 1 and 2, Figures S3 and S4), and the $J_{\text{P-H(Me)}}$ values of II and III are very similar to that of $\text{C}_5\text{H}_4\text{PMePh}_2$.^{3a}

Ruthenium Complex Syntheses and NMR Characterization. Ruthenium coordination complexes of the three phosphonium-1-indenylides were obtained via substitution reactions of the labile complex $[\text{Ru}(\eta^5\text{-C}_5\text{H}_5)(\text{MeCN})_3]\text{PF}_6$ ⁸ (eq 1).



The reactions were generally completed within a few minutes on stirring equimolar amounts of $[\text{Ru}(\eta^5\text{-C}_5\text{H}_5)(\text{MeCN})_3]\text{PF}_6$ and a PHIN ligand in THF at room temperature, and crystallographic quality crystals of the complexes $[\text{Ru}(\eta^5\text{-C}_5\text{H}_5)(\eta^5\text{-}1\text{-C}_9\text{H}_6\text{PPh}_3)]\text{PF}_6$ (IV), $[\text{Ru}(\eta^5\text{-C}_5\text{H}_5)(\eta^5\text{-}1\text{-C}_9\text{H}_6\text{PMePh}_2)]\text{PF}_6$ (V), and $[\text{Ru}(\eta^5\text{-C}_5\text{H}_5)(\eta^5\text{-}1\text{-C}_9\text{H}_6\text{PMe}_2\text{Ph})]\text{PF}_6$ (VI) were obtained by slow evaporation from saturated CH_2Cl_2 solutions (see below). Unfortunately, bulk purification of the complexes was not readily accomplished, as attempted recrystallization from a variety of solvents and solvent mixtures generally failed to produce pure materials. Washing the products with benzene was found to remove some nonpolar impurities but, judging from the elemental analyses and the ^1H NMR spectra, attempts to remove of all traces of impurities were generally unsuccessful.

Nonetheless, complexes IV–VI were all unambiguously characterized as such by X-ray crystallography, by electrospray mass spectrometry, and by ^1H , ^{31}P , and ^{13}C NMR spectroscopy. Crystal structures of the three compounds are discussed below, while experimental and simulated ES mass spectra of VI are shown in Figure 9 and those of IV and V in Figure S5 of the Supporting Information. The isotopic patterns observed for all three complex cations are in excellent agreement with the calculated spectra.

Chemical shift and coupling constant data are given in Tables 1–3, comparisons with the corresponding data for the free PHIN ligands being readily obvious. The ^1H spectrum of VI is shown in Figure 10 and those of IV and V are shown respectively in Figures S6 and S7 of the Supporting Information.

Of specific interest, coordination of the three planar-prochiral PHIN ligands resulted in the formation of enantiomeric pairs, depending on which face of the five-membered rings coordinates (as in Figure 3). The result is that the methyl groups of VI and the phenyl groups of V are diastereotopic, as with regioisomer a of the phosphonium salts $(1\text{-C}_9\text{H}_7\text{PMe}_2\text{Ph})\text{Br}$ and $(1\text{-C}_9\text{H}_7\text{PMePh}_2)\text{Br}$, respectively (see above). Therefore, in contrast to the ^1H NMR spectrum of free $1\text{-C}_9\text{H}_7\text{PMe}_2\text{Ph}$ (III; Figure 8), the ^1H NMR spectrum of VI exhibited two methyl resonances (Figure 10) while that of IV exhibited two sets of phenyl resonances (although these were difficult to distinguish). A corollary of these findings is, of course, that inter- and intramolecular interfacial exchange of the coordinated PHIN ligands (enantiomeric exchange) must be slow on at least the NMR time scale.

As is also clear from Tables 1–3 and Figures 8 and 10 and Figures S3, S4, S6, and S7, formation of complexes IV–VI results in significant upfield coordination shifts of the resonances of H(2) and H(3), about 2 and 1 ppm, respectively. Very similar coordination shifts were observed for the compound $\text{Cr}(\eta^5\text{-}1\text{-C}_9\text{H}_6\text{PMePh}_2)(\text{CO})_3$ ⁴ and also for H(2,5) and H(3,4) of the five-membered rings in the group 6 methylidiphenylphosphonium cyclopentadienylide complexes $\text{M}(\eta^5\text{-C}_5\text{H}_4\text{PMePh}_2)(\text{CO})_3$ (M = Cr, Mo, W).^{3a} In contrast, the resonances of H(5)–H(8) and of the phenyl groups in the NMR spectra of compounds IV–VI change relatively little, consistent with metal–ylide bonding involving only the five-membered rings.

Table 1. ^1H and ^{13}C NMR Data for I and IV

H, C position	I		IV	
	$\delta(^1\text{H})$	$\delta(^{13}\text{C})$	$\delta(^1\text{H})$	$\delta(^{13}\text{C})$
1		66.52 (d, $^1J_{\text{P-C}} = 123$)		57.7 (d, $^1J_{\text{C-P}} = 104.8$ Hz)
2	6.61 (t, $J_{\text{H-H}} = J_{\text{P-H}} = 4.53$)	128.2 (d, $^3J_{\text{P-C}} = 16.0$)	4.66 (s)	79.2 (d, $^2J_{\text{C-P}} = 14.5$ Hz)
3	6.56 (t, $J_{\text{H-H}} = J_{\text{P-H}} = 4.16$)	106.4 (d, $^2J_{\text{P-C}} = 16.0$)	5.86 (s)	71.6 (d, $^3J_{\text{C-P}} = 11.2$ Hz)
4		135.7 (d, $^2J_{\text{P-C}} = 13.5$)		96.2 (d, $^3J_{\text{C-P}} = 12.3$ Hz)
5	7.66 (? , obscured)	120.4 (s)	6.84 (d, $^3J_{\text{H-H}} = 8.9$ Hz)	123.6 (s)
6	6.95 (t, $^3J_{\text{H-H}} = 7.18$)	117.7 (s)	7.03 (td, $^3J_{\text{H-H}} = 7.3$ Hz)	127.1 (s)
7	6.76 (t, $^3J_{\text{H-H}} = 7.18$)	118.0 (s)	7.14 (td, $^3J_{\text{H-H}} = 7.7$ Hz)	126.0 (s)
8	6.89 (d, $^3J_{\text{H-H}} = 7.93$)	117.2 (s)	7.67 (d, $^3J_{\text{H-H}} = 8.5$ Hz)	127.7 (s)
9		137.8 (d, $^3J_{\text{P-C}} = 14.8$)		97.7 (d, $^2J_{\text{C-P}} = 9.7$ Hz)
<i>ipso-C</i>		125.8 (d, $^1J_{\text{P-C}} = 89.8$)		120.3 (d, $^1J_{\text{C-P}} = 92.2$ Hz)
<i>o-C</i>	7.68–7.65 (m)	133.8 (d, $^3J_{\text{P-C}} = 9.84$)	7.82 (m)	134.4 (d, $^2J_{\text{C-P}} = 10.9$ Hz)
<i>m-C</i>	7.51 (td, $J_{\text{H-H}} = 3.02, 7.93$)	129.1 (d, $^2J_{\text{P-C}} = 12.3$)	7.76 (m)	130.6 (d, $^3J_{\text{C-P}} = 12.4$ Hz)
<i>p-C</i>	7.62 (t, $^3J_{\text{H-H}} = 7.55$)	133.6 (d, $^4J_{\text{P-C}} = 3.7$)	8.00 (m)	135.8 (d, $^4J_{\text{C-P}} = 3.8$ Hz)
C_5H_5			4.35 (s)	73.8 (s)

Table 2. ^1H and ^{13}C NMR Data for II and V

H, C position	II		V	
	$\delta(^1\text{H})$	$\delta(^{13}\text{C})$	$\delta(^1\text{H})$	$\delta(^{13}\text{C})$
1		66.14 (d, $^1J_{\text{P-C}} = 120.8$)		58.2 (d, $^1J_{\text{C-P}} = 103.4$ Hz)
2	6.74 (t, $J_{\text{H-H}} = J_{\text{P-H}} = 4.5$)	126.30 (d, $^2J_{\text{P-C}} = 17.6$)	4.64 (s)	77.8 (d, $^2J_{\text{C-P}} = 14.4$ Hz)
3	6.46 (t, $J_{\text{H-H}} = J_{\text{P-H}} = 4.2$)	105.00 (d, $^3J_{\text{P-C}} = 15.4$)	5.79 (s)	70.9 (d, $^1J_{\text{C-P}} = 9.6$ Hz)
4		135.42 (d, $^2J_{\text{P-C}} = 14.3$)		94.3 (d, $^3J_{\text{C-P}} = 13.2$ Hz)
5	7.68 (m)	120.82 (s)	7.59 (t, $^3J_{\text{H-H}} = 8.9$ Hz)	126.7 (s)
6	6.97 (t, $^3J_{\text{H-H}} = 7.2$)	117.28 (s)	6.93 (d, $^3J_{\text{H-H}} = 8.0$ Hz)	123.1 (s)
7	6.84 (t, $^3J_{\text{H-H}} = 6.8$)	117.91 (s)	7.08 (d, $^3J_{\text{H-H}} = 7.9$ Hz)	125.4 (s)
8	7.04 (d, $^3J_{\text{H-H}} = 7.9$)	117.36 (s)	6.98 (d, $^3J_{\text{H-H}} = 6.0$ Hz)	126.2 (s)
9		137.79 (d, $^3J_{\text{P-C}} = 15.4$)		97.0 (d, $^2J_{\text{C-P}} = 8.2$ Hz)
P-Me	2.50 (d, $^2J_{\text{P-H}} = 12.6$)	12.97 (d, $^1J_{\text{P-C}} = 62.6$)	2.88 (d, $^2J_{\text{P-H}} = 13.3$ Hz)	13.3 (d, $^1J_{\text{C-P}} = 61.9$ Hz)
<i>ipso-C</i>		127.13 (d, $^1J_{\text{P-C}} = 87.8$)		119.8 (d, $^1J_{\text{C-P}} = 40.8$ Hz)
<i>o-C</i>	7.55–7.52	129.45 (d, $^2J_{\text{P-C}} = 12.1$)	7.71 (m)	132.6 (d, $^2J_{\text{C-P}} = 10.9$ Hz)
<i>m-C</i>	7.67–7.63	132.68 (d, $^3J_{\text{P-C}} = 11.0$)	7.64 (m)	130.1, 130.3 (d, $^3J_{\text{C-P}} = 12.8$ Hz)
<i>p-C</i>	7.67–7.53	132.93 (d, $^4J_{\text{P-C}} = 3.3$)	7.83 (dd, $J_{\text{H-H}} = 8.9$ Hz)	135.1, 135.2 (d, $^4J_{\text{C-P}} = 3.2$ Hz)
C_5H_5			4.45 (s)	73.2

Table 3. ^1H and ^{13}C NMR Data for III and VI

H, C position	III		VI	
	$\delta(^1\text{H})$	$\delta(^{13}\text{C})$	$\delta(^1\text{H})$	$\delta(^{13}\text{C})$
1		66.69 (d, $^1J_{\text{P-C}} = 121$)		58.4 (d, $^1J_{\text{P-C}} = 102$)
2	6.98 (t, $J_{\text{H-H}} = J_{\text{P-H}} = 4.53$)	124.2 (d, $^2J_{\text{P-C}} = 16.5$)	5.00 (s)	77.0 (d, $^2J_{\text{P-C}} = 14.5$)
3	6.64 (t, $J_{\text{H-H}} = J_{\text{P-H}} = 4.53$)	105.8 (d, $^3J_{\text{P-C}} = 14.8$)	5.83 (s)	71.5 (d, $^3J_{\text{P-C}} = 9.6$)
4		134.4 (d, $^2J_{\text{P-C}} = 14.8$)		94.3 (d, $^3J_{\text{P-C}} = 14.5$)
5	7.68 (d, $^3J_{\text{H-H}} = 8.69$)	120.6 (d, $^4J_{\text{P-C}} = 1.85$)	7.61 (d, $^3J_{\text{H-H}} = 8.38$)	126.8 (s)
6	6.95 (t, $^3J_{\text{H-H}} = 7.55$)	116.9 (s)	7.13 (d, $^3J_{\text{H-H}} = 7.50$)	125.9 (s)
7	6.87 (t, $^3J_{\text{H-H}} = 7.55$)	117.6 (s)	7.10 (d, $^3J_{\text{H-H}} = 7.50$)	125.7 (s)
8	7.18 (d, $^3J_{\text{H-H}} = 7.93$)	116.8 (d, $^3J_{\text{P-C}} = 1.85$)	7.21 (d, $^3J_{\text{H-H}} = 8.52$)	123.1 (s)
9		137.1 (d, $^2J_{\text{P-C}} = 13.0$)		97.3 (d, $^2J_{\text{P-C}} = 8.0$)
P-Me	2.21 (d, $^2J_{\text{P-H}} = 13.2$)	12.92 (d, $^2J_{\text{P-C}} = 61.0$)	2.70 (d, $^2J_{\text{P-H}} = 13.2$), 2.44 (d, $^2J_{\text{P-H}} = 13.2$)	11.8 (d, $^2J_{\text{P-C}} = 62.1$), 13.7 (d, $^2J_{\text{P-C}} = 62.1$)
<i>ipso-C</i>		128.3 ($^1J_{\text{P-C}} = 84.2$)		121.4 ($^1J_{\text{P-C}} = 86.5$)
<i>o-C</i>	7.64 (dd, $J_{\text{H-H}} = 7.30, 13.0$)	131.0 (d, $^2J_{\text{P-C}} = 11.1$)	7.77 (dd, $J_{\text{H-H}} = 5.58, 12.71$)	131.5 (d, $^3J_{\text{P-C}} = 10.6$)
<i>m-C</i>	7.49 (td, $J_{\text{H-H}} = 2.27, 7.56$)	129.3 (d, $^3J_{\text{P-C}} = 12.0$)	7.67 (td, $J_{\text{H-H}} = 3.25, 7.59$)	130.6 (d, $^2J_{\text{P-C}} = 12.4$)
<i>p-C</i>	7.58 (t, $J_{\text{H-H}} = 7.93$)	132.6 (d, $^4J_{\text{P-C}} = 2.77$)	7.37 (m)	135.1 (d, $^4J_{\text{P-C}} = 3.1$)
C_5H_5			4.51 (s)	73.2 (s)

We note that the $\eta^5\text{-C}_5\text{H}_5$ resonances of complexes IV (δ 4.35), V (δ 4.45), and VI (δ 4.55) correlate with the electron-donating abilities of the PHIN ligands expected on the basis of

the substituents on phosphorus and are all somewhat deshielded relative to the corresponding resonance of their precursor, $[\text{Ru}(\eta^5\text{-C}_5\text{H}_5)(\text{MeCN})_3]\text{PF}_6$ (δ 4.29). The ^{31}P

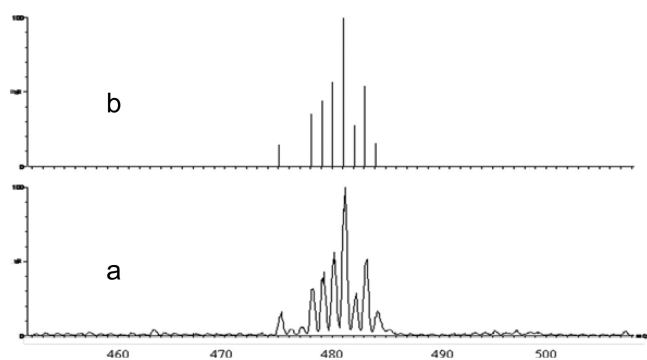


Figure 9. Experimental (a) and simulated (b) mass spectra of VI.

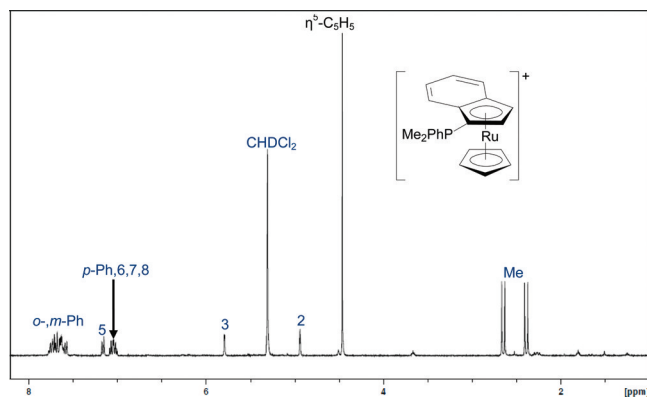


Figure 10. ^1H NMR spectrum of $[\text{Ru}(\eta^5\text{-C}_5\text{H}_5)(\eta^5\text{-1-C}_9\text{H}_6\text{PMe}_2\text{Ph})]\text{PF}_6$ (VI).

chemical shifts of I–VI are δ 1.60, 4.83, 10.4, 22.4, 23.3, and 24.3, respectively, and thus coordination of the ylides to Ru(II) results in downfield coordination shifts of about 14–21 ppm. These changes compare with downfield shifts of \sim 14 ppm for $\text{Cr}(\eta^5\text{-1-C}_9\text{H}_6\text{PMePh}_2)(\text{CO})_3$ ⁴ and 10–12 ppm for the compounds $\text{M}(\eta^5\text{-C}_5\text{H}_4\text{PMePh}_2)(\text{CO})_3$ ($\text{M} = \text{Cr}, \text{Mo}, \text{W}$).^{3a}

Crystallographic Characterization of Ligands and Ruthenium Complexes. X-ray-quality crystals of I and III were obtained by recrystallization from CH_2Cl_2 solution layered with hexanes, and the structures are shown in Figures 11 and 12, respectively. Similarly, crystals of compounds IV–VI

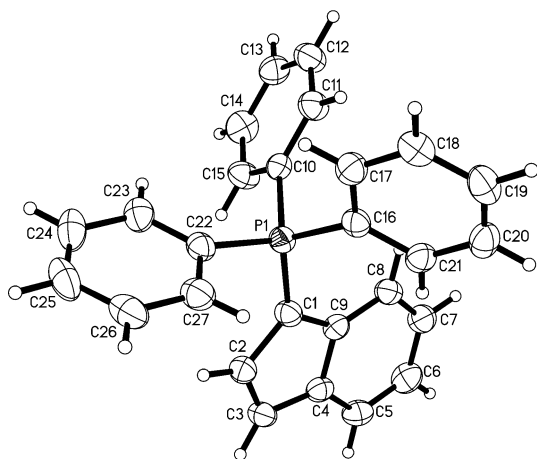


Figure 11. Molecular structure of $1\text{-C}_9\text{H}_6\text{PPh}_3$ (I). Displacement ellipsoids for non-H atoms are shown at the 50% probability level, and H atoms are represented by circles of arbitrary size.

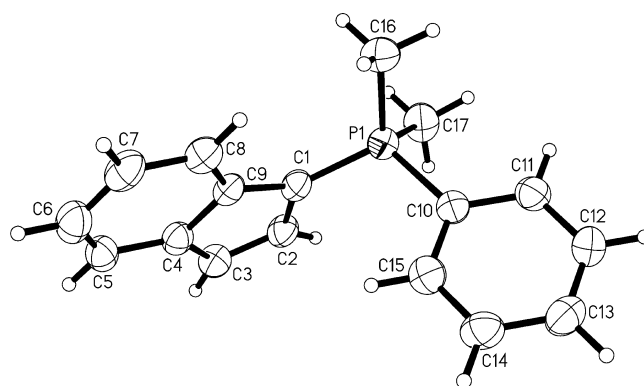


Figure 12. Molecular structure of $1\text{-C}_9\text{H}_6\text{PPh}_3$ (III). Displacement ellipsoids for non-H atoms are shown at the 50% probability level, and H atoms are represented by circles of arbitrary size.

were obtained by slow evaporation of saturated CH_2Cl_2 solutions and the structures are shown in Figures 13–15,

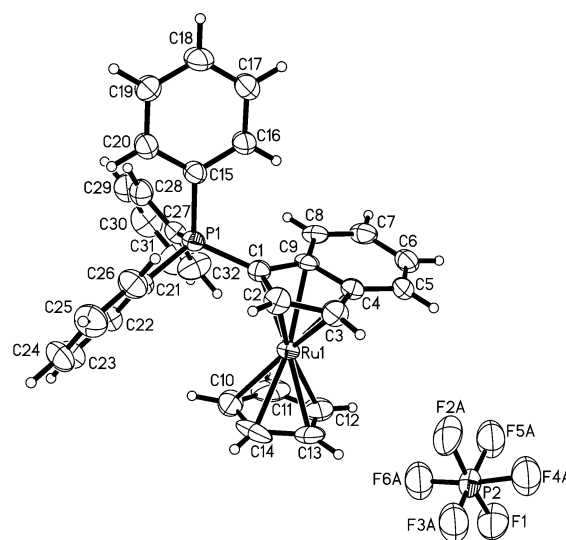


Figure 13. Molecular structure of $[\text{Ru}(\eta^5\text{-C}_5\text{H}_5)(\eta^5\text{-1-C}_9\text{H}_6\text{PPh}_3)]\text{PF}_6$ (IV). Displacement ellipsoids for non-H atoms are shown at the 50% probability level, and H atoms are represented by circles of arbitrary size.

respectively. Important bond lengths and angles for compounds I–VI are shown in Table 4, and full crystallographic information is available in the Supporting Information.

With reference to Figure 2, an important structural parameter for assessing the relative contributions of the resonance structures a and b to the overall electronic structure involves the bond lengths and angles of the 1-indenyl-P moiety. The P– C_9H_6 bond lengths of I–III are respectively 1.7284(19), 1.711(2), and 1.727(3) Å, all significantly shorter than the corresponding P–Ph bonds. The latter average 1.810, 1.788, and 1.817 Å, respectively, all falling within the typical range for C–Ph single bonds in phenyl phosphonium ylides.⁹ On the other hand, the P– C_9H_6 bond lengths of I–III are significantly longer than the P=CH₂ bond in $\text{Ph}_3\text{P}=\text{CH}_2$ (1.66 Å);⁹ the latter is a typical example of a non-resonance-stabilized ylide, and its P=CH₂ bond is believed to contain considerable double-bond character.^{9a} Thus, the P– C_9H_6 bond lengths of I–III are consistent with significant contributions from both the

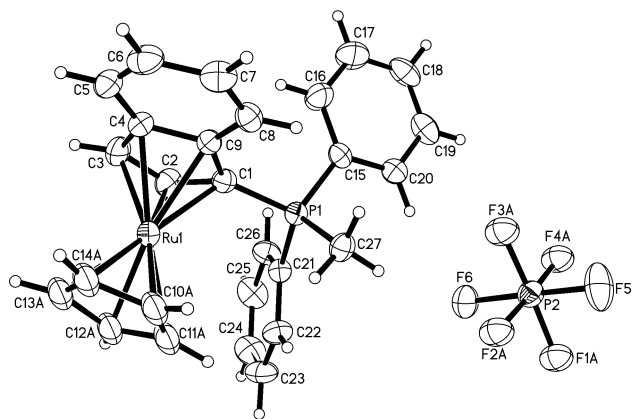


Figure 14. Molecular structure of $[\text{Ru}(\eta^5\text{-C}_5\text{H}_5)(\eta^5\text{-1-C}_5\text{H}_4\text{PMePh}_2)]\text{PF}_6$ (V). Displacement ellipsoids for non-H atoms are shown at the 50% probability level, and H atoms are represented by circles of arbitrary size.

uncharged and the zwitterionic resonance structures **a** and **b** in Figure 2.

Interestingly, although the C–C–C bond angles within the five-membered rings of all three ylides are all very close to the 108° of a regular pentagon, moderately alternating patterns of the C–C bond lengths seemingly provide evidence for a degree of localization of π bond electron density. Thus, the C(2)–C(3), C(5)–C(6), and C(7)–C(8) bonds of all three ligands are “short” and the C(1)–C(2), C(3)–C(4), C(4)–C(5), C(6)–C(7), and C(8)–C(9) bonds are “long”, as in **a** and **b** of Figure 2. Thus, again there is evidence for a very significant contribution from both the uncharged and the zwitterionic resonance structures, although the C(4)–C(9) bonds are “long”, as is the case with the analogous bond of naphthalene.^{10a}

The complexes **IV–VI** all assume sandwich structures, as anticipated. The five-membered rings are almost exactly eclipsed in all cases, and the phosphine moieties are oriented such that a phenyl group is always trans to the $\eta^5\text{-C}_5\text{H}_5$ ligand while the other two groups (Me, Ph) straddle the $\eta^5\text{-C}_5\text{H}_5$ ligand. The bond length alternation of the C(5)–C(6), C(6)–C(7), and C(7)–C(8) bonds of the six-membered ring becomes more pronounced on coordination, but the C(2)–C(3) bonds lengthen such that the C–C bond lengths of the five-membered rings are all rather similar, with the average being $\sim 1.44 \pm 0.02 \text{ \AA}$. The P–C₉H₆ bond lengths also increase

somewhat on coordination, and thus the zwitterionic structure **b** apparently becomes more significant in the complexes than is the case for the free ligands. Similar behavior was observed with group 6 metal compounds of $\text{C}_5\text{H}_4\text{PMePh}_2$ and $1\text{-C}_9\text{H}_6\text{PMePh}_2$ ^{3,4} and presumably reflects enhanced aromatization of the cyclopentadienyl-like ligands on coordination to the low-spin d^6 metal systems.

There are, however, marked differences in the lengths of the bonds between the ruthenium atoms and the ylidic carbon atoms of complexes **IV–VI**. While the Ru–C(1), Ru–C(2), and Ru–C(3) bond lengths are similar in each case and only slightly longer (averages 2.17–2.19 Å) than the averages of the Ru–C₅H₅ bond lengths, the Ru–C(4) and Ru–C(9) bonds are significantly longer (averages 2.23–2.25 Å). Similar behavior was observed with the aforementioned $\text{C}_5\text{H}_4\text{PMePh}_2$ and $1\text{-C}_9\text{H}_6\text{PMePh}_2$ group 6 metal compounds.^{3,4} As a result of these differences, the five-membered ylidic rings of **IV–VI** are tilted at angles of 5.63, 6.90, and 4.94° , respectively, relative to the corresponding C₅H₅ rings.

Somewhat similar behavior is also observed in many complexes containing coordinated indenyl ligands, where indenyl “slippage” to what is essentially an η^3 allyl-ene mode of bonding is observed.^{10b} In these cases, however, there is considerable loss of planarity of the indenyl moiety such that the angle between the C(1)–C(2)–C(3) plane and the C(1)–C(3)–C(4)–C(9) plane (the hinge angle) is typically $20\text{--}30^\circ$ while the angle between the C(1)–C(2)–C(3) plane and the C(4)–C(5)–C(6)–C(7)–C(8)–C(9) plane (the fold angle) is typically $>12^\circ$.^{10b} In **IV–VI**, the hinge and fold angles are $2.91\text{--}3.72$ and $4.32\text{--}5.89^\circ$, respectively, much more typical of essentially planar η^5 -indenyl complexes.^{10b}

Computational Studies. For purposes of comparison and to gain insight into the nature of the metal–ligand bonding, we have calculated structures for the free ligands $\text{C}_5\text{H}_4\text{PMe}_3$, $\text{C}_5\text{H}_4\text{PF}_3$, $1\text{-C}_9\text{H}_6\text{PMePh}_2$ (**II**), $1\text{-C}_9\text{H}_6\text{PMe}_2\text{Ph}$ (**III**), $1\text{-C}_9\text{H}_6\text{PF}_3$, and C_6H_6 , as well as for their corresponding $[\text{Ru}(\eta^5\text{-C}_5\text{H}_5)]^+$ complexes. Geometries were optimized at the b3-lyp/TZVP level, and improved single-point energies were calculated at the b3-lyp/TZVPP level. Listings of the Cartesian coordinates are available in the Supporting Information (Table S1).

The calculated geometries of both the $1\text{-C}_9\text{H}_6$ ligands and their complexes (Table 5) agree well with the observed X-ray structures. In particular, the free ligands all show a “short”

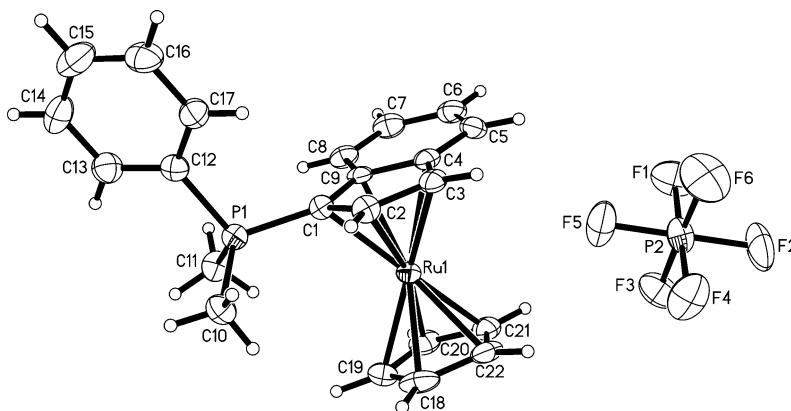


Figure 15. Molecular structure of $1\text{-C}_9\text{H}_6\text{PPh}_3$ (VI). Displacement ellipsoids for non-H atoms are shown at the 50% probability level, and H atoms are represented by circles of arbitrary size.

Table 4. Selected Bond Lengths (Å) and Angles (deg) for Compounds I–VI^a

	I	II	III	IV	V	VI
P(1)–C(1)	1.7284(19)	1.711(2)	1.727(3)	1.768(5)	1.763(3)	1.761(4)
P–Me		1.787(2)	1.785(4)		1.787(3)	1.786
P–Ph av	1.8100	1.788	1.817(3)	1.794	1.790	1.787(4)
C(1)–C(2)	1.427(3)	1.420(3)	1.424(4)	1.444(7)	1.443(5)	1.446(5)
C(2)–C(3)	1.368(3)	1.364(3)	1.374(5)	1.411(8)	1.412(5)	1.414(5)
C(3)–C(4)	1.429(3)	1.421(3)	1.417(5)	1.418(7)	1.427(5)	1.435(6)
C(4)–C(5)	1.406(3)	1.397(3)	1.411(5)	1.427(7)	1.431(5)	1.423(6)
C(5)–C(6)	1.374(3)	1.362(3)	1.368(5)	1.350(8)	1.351(6)	1.365(6)
C(6)–C(7)	1.399(3)	1.394(3)	1.407(5)	1.422(8)	1.427(5)	1.415(6)
C(7)–C(8)	1.372(3)	1.369(3)	1.372(5)	1.355(7)	1.356(5)	1.367(6)
C(8)–C(9)	1.406(3)	1.400(3)	1.416(5)	1.420(7)	1.423(5)	1.423(5)
C(4)–C(9)	1.438(3)	1.423(3)	1.437(4)	1.445(7)	1.435(5)	1.439(6)
C(1)–C(9)	1.435(3)	1.432(3)	1.435(4)	1.459(7)	1.457(5)	1.449(6)
C(1)–Ru				2.163(5)	2.170(3)	2.151(4)
C(2)–Ru				2.176(5)	2.172(4)	2.163(4)
C(3)–Ru				2.176(5)	2.183(4)	2.187(4)
C(4)–Ru				2.220(5)	2.230(4)	2.257(4)
C(9)–Ru				2.240(5)	2.242(3)	2.246(4)
C ₅ H ₅ –Ru av				2.16	2.17	2.17
C(1)–P–Me		111.9(10)	112.12		111.38(17)	110.8
C(1)–P–Ph av	110.80	111.16	112.31(15)	110.0	109.2	109.95(19)
Me–P–Ph av		107.0	106.19		109.5	108.0
Ph–P–Ph av	110.47	108.33		108.9	107.9	
C(1)–C(2)–C(3)	110.12(17)	110.1(2)	110.1(3)	108.5	108.6(3)	108.0(3)
C(2)–C(3)–C(4)	108.50(18)	108.2(2)	108.2(3)	108.8(5)	108.5(3)	108.5(3)
C(3)–C(4)–C(9)	107.47(17)	107.96(19)	108.1(3)	108.8(5)	108.6(3)	108.6(4)
C(4)–C(9)–C(1)	107.22(16)	107.09(18)	107.0(3)	106.5(4)	107.0(3)	106.8(3)
C(9)–C(1)–C(2)	106.67(16)	106.64(19)	106.6(3)	107.3(5)	107.2(3)	108.0(3)

^aData for II are from ref 4.Table 5. Calculated C–C Bond Lengths (Å) for C₅H₄ and 1-Indenylidene Ligands and Their Complexes

ligand	free ylide			[Ru(η ⁵ -ylidene)(η ⁵ -C ₅ H ₅)] ⁺		
	C(2)–C(3)	av C–C ^a	rms dev ^b	C(2)–C(3)	av C–C ^a	rms dev ^b
C ₅ H ₄ PMe ₃	1.387	1.419	0.021	1.421	1.434	0.011
C ₅ H ₄ PF ₃	1.370	1.428	0.038	1.415	1.439	0.019
1-C ₉ H ₆ PMe ₃	1.376	1.437	0.025	1.417	1.447	0.014
1-C ₉ H ₆ PMe ₂ Ph	1.376	1.438	0.025	1.417	1.447	0.014
1-C ₉ H ₆ PMePh ₂	1.375	1.439	0.026	1.417	1.447	0.014
1-C ₉ H ₆ PPh ₃	1.375	1.439	0.026	1.416	1.448	0.015
1-C ₉ H ₆ PF ₃	1.360	1.449	0.038	1.410	1.452	0.020

^aExcluding C(2)–C(3). ^bAll C–C.

C(2)–C(3) bond of 1.37 Å while the other bonds in the five-membered ring are all rather similar (1.42–1.44 Å). Coordination of the ligands to [Ru(η⁵-C₅H₅)]⁺ results in “equalization” of the ring bonds, reducing the rms deviation from the average ring C–C bond length by a factor of about 2, which can be taken as evidence for the increased contribution of resonance structure **b** in the ruthenium complexes.

The optimized geometries also reflect the difference in Ru–C bond lengths for the five-membered rings: Ru–C(4) and Ru–C(9) are systematically about 0.1 Å longer than the other three Ru–C bonds, in contrast to the rather symmetrical bonding of C₅H₄PR₃ to [Ru(η⁵-C₅H₅)]⁺. Comparisons of the relevant ligand donor orbitals of C₅H₄PR₃ and 1-indenylidenePR₃ (see Figure 16) help to explain these trends. Donation from the pair of orbitals HOMO, HOMO-1 is likely to be equally effective for corresponding C₅H₄PR₃ and (1-indenylidene)PR₃

ligands and would not result in very different bonding to individual carbons. For C₅H₄PR₃, the lower lying HOMO-2 is also more or less evenly spread out over the C₅H₄ ring and, as a result, the ruthenium complex shows nearly symmetrical bonding (rms deviation 0.017 Å). In contrast, the corresponding (1-indenylidene)PMe₃ HOMO-3 orbital is primarily concentrated on C(1)–C(3), and hence [Ru(η⁵-C₅H₅)]⁺ binds more strongly to these three carbons than to the remaining two (rms deviation 0.04–0.05 Å).

The X-ray structures of complexes IV–VI exhibit some tilting of the two five-membered rings (η⁵-C₅H₅ and η⁵-1-C₉H₆) relative to each other. The calculated tilt angles between the two least-squares ring planes, 4–7° for the C₅H₄PMe₃ and (1-indenylidene)PMe_xPh_{3-x} complexes, are essentially identical with those observed. The tilting probably occurs because

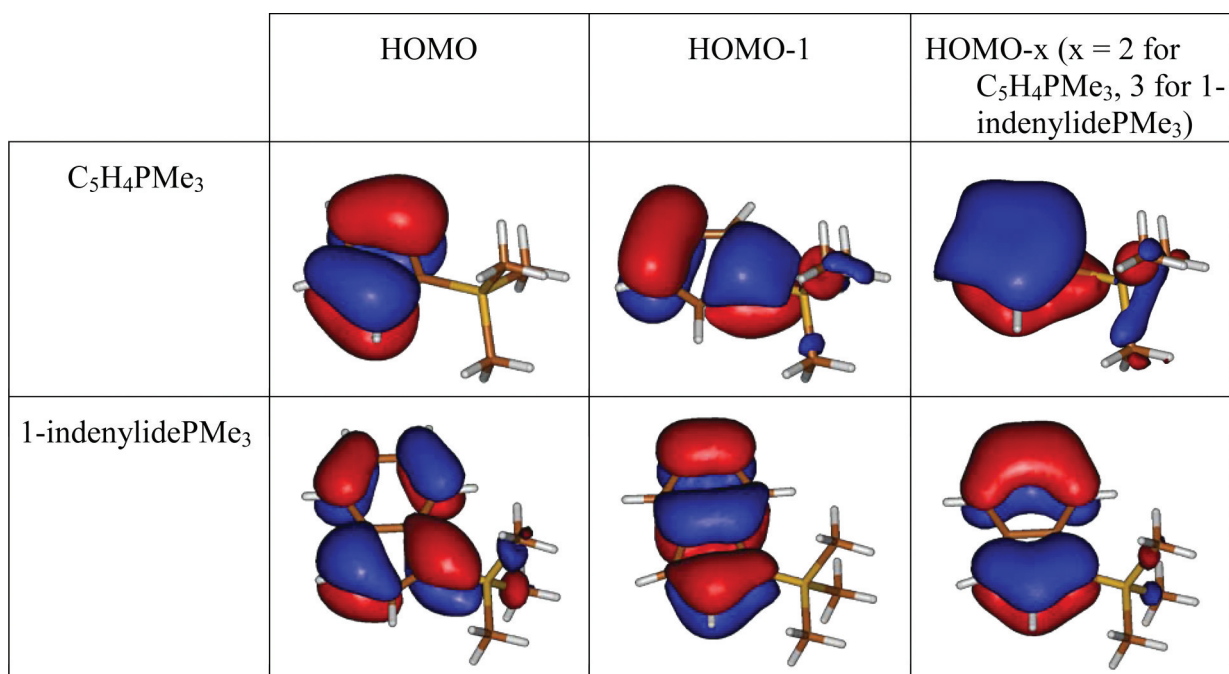


Figure 16. Donor orbitals of the ligands C₅H₄PMe₃ and 1-indenylydePMe₃.

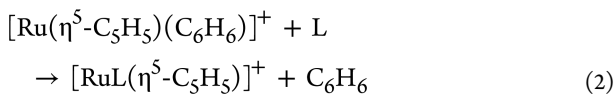
neither the C₅H₄PR₃ nor the (1-indenylyde)PR₃ ligands bind in electronically symmetrical fashions to the metal.

Table 6. Complex Stabilities (kcal/mol) Relative to C₆H₆

ligand	ΔG_{273}^a
C ₅ H ₄ PMe ₃	-32.8
C ₅ H ₄ PF ₃	-6.1
1-C ₉ H ₆ PMe ₃	-19.0
1-C ₉ H ₆ PMe ₂ Ph	-20.6
1-C ₉ H ₆ PMePh ₂	-22.6
1-C ₉ H ₆ PPh ₃	-20.4
1-C ₉ H ₆ PF ₃	4.7

^a ΔG for reaction 2, calculated for gas phase, 1 bar, 273 K, but entropy scaled by 0.67 to correct for reduced freedom in solution.

Given in Table 6 are calculated complex stabilities (ΔG_{273}) relative to benzene, i.e. the free-energy change of the reaction



In agreement with a trend noted in earlier work on isoelectronic Cr(CO)₃ complexes,^{3,4} C₅H₄PMe₃ was found to be a much stronger donor than benzene (by about 33 kcal/mol). As expected, introduction of electronegative fluorine substituents on phosphorus strongly reduces the coordinating power of the ligand (by 25 kcal/mol), presumably because of inductive effects. Turning now to the 1-indenylyde ligands, the data in Table 6 demonstrate that these bind more weakly to [Ru(η^5 -C₅H₅)]⁺ than their cyclopentadienyl analogues by about 14 kcal/mol. A reasonable explanation is that one π orbital is less available for donation to ruthenium because of competing mixing with the benzene ring π orbitals (HOMO-*x*; see Figure 16). Again, introduction of fluorines on phosphorus reduces the ligand binding energy by about 25 kcal/mol, leading now to a ligand that binds more weakly to [Ru(η^5 -C₅H₅)]⁺ than

does benzene. Replacement of the methyl groups at phosphorus by phenyl groups might also be expected to reduce the metal–ligand bond strength, since phenyl is more electron withdrawing than is methyl, but we see no evidence of this. In fact, the metal–ligand bond strengths *increase* by 2 kcal/mol for each of the first two Ph groups and then only decrease by 2 kcal/mol for the third because of steric factors. It should be noted that these calculations were done for gas-phase ions, and the possibility of more extensive delocalization of the positive charge may have artificially stabilized the more phenylated species. Perhaps the safest conclusion is that the replacement of methyl by phenyl groups has at most a very modest effect on the ligand binding strength.

CONCLUSIONS

A series of aromatic phosphonium-1-indenylyde (PHIN) ligands and the corresponding ruthenium complexes [Ru(η^5 -C₅H₅)(η^5 -1-C₉H₆PPh₃)]PF₆, [Ru(η^5 -C₅H₅)(η^5 -1-C₉H₆PMePh₂)]PF₆, and [Ru(η^5 -C₅H₅)(η^5 -1-C₉H₆PMe₂Ph)]PF₆ have been synthesized and characterized by ¹H, ¹³C, and ³¹P NMR spectroscopy, by X-ray crystallography, and by extensive DFT calculations. The calculations produce optimized geometries consistent with the crystallographic data and suggest that PHIN ligands bind considerably more strongly to ruthenium(II) than do analogous arene ligands. Consistent with this conclusion, NMR data show that interconversion of enantiomers via interfacial exchange of the η^5 -bound ligands does not occur: i.e., the complexes exhibit configurational stability. Applications exploiting the planar chirality of the complexes can be expected.

EXPERIMENTAL SECTION

All syntheses were carried out under dry, deoxygenated argon using standard Schlenk line techniques. Argon was deoxygenated by passage through a heated column of BASF copper catalyst and then dried by passing through a column of activated 4A molecular sieves. NMR spectra were recorded using a Bruker AV600 spectrometer, ¹H and ¹³C

NMR data being referenced to TMS via the residual protons signals of the deuterated solvent. $[\text{Ru}(\eta^5\text{-C}_5\text{H}_5)(\text{MeCN})_3]\text{PF}_6$, was purchased from Strem Chemicals, while 1-bromoindene was prepared via cleavage of the carbon–silicon bond of 1-trimethylsilylindene by dioxane dibromide.⁷

Syntheses of the Phosponium Salts (1-C₉H₇PPh₃)Br, (1-C₉H₇PMePh₂)Br and (1-C₉H₇PMe₂Ph)Br. In a typical reaction, a solution of 3.5 g of 1-bromoindene and 5.14 g of PPh₃ (1:1 molar ratio) in 50 mL of toluene was heated at 50 °C for 72 h to give a white precipitate of the phosponium salt $[\text{1-C}_9\text{H}_7\text{PPh}_3]\text{Br}$. The product was collected by filtration and dried under reduced pressure (4.0 g, 49% yield). Anal. Calcd for C₂₇H₂₂PBr: C, 70.95; H, 4.85. Found: C, 70.43; H, 4.93. The ¹H NMR spectrum is shown in Figure S1 (Supporting Information), while a ³¹P NMR spectrum (CD₂Cl₂) exhibited resonances at δ 12.5 (isomer A) and 26.6 (isomer B) in a 3:1 ratio.

In a similar manner, a white, air-sensitive precipitate of (1-C₉H₇PMePh₂)Br was prepared (8.90 g, 88% yield) by stirring a solution of 4.84 mL of PMePh₂ (25.7 mmol) and 5.03 g 1-bromoindene (25.7 mmol) in 75 mL of toluene for 24 h at room temperature. ¹H NMR (Figure S2 (Supporting Information)) and ³¹P NMR spectra (CD₂Cl₂) showed that the material was a mixture of regioisomers (Figure 7). ¹H NMR (CD₂Cl₂, 500 MHz): δ 3.9 (br s, CH₂CCH=C of isomer A), 3.1 (d, PCH₃ of isomer A, ²J_{P-H} = 13.1 Hz), 2.8 (d, PCH₃ of isomer B, ²J_{P-H} = 13.1 Hz). ³¹P NMR (CD₂Cl₂): δ 13.6 (isomer A), 25.9 (isomer B). The relative intensities of the ¹H doublets and the ³¹P singlets indicated for this sample a 42:58 ratio of isomer A to isomer B.

In a similar fashion, a solution of 2.13 mL of PMe₂Ph (15 mmol) and 2.93 g of 1-bromoindene (15 mmol) in 50 mL of toluene was stirred for 24 h at room temperature to yield white, air-sensitive (1-C₉H₇PMe₂Ph)Br (2.40 g, 48% yield). Anal. Found for C₁₇H₁₈PBr: C, 58.97; H, 4.99. Calcd: C, 61.28; H, 5.44. ¹H NMR (Figure 2) and ³¹P NMR spectra (CD₂Cl₂) showed that the material was a mixture of regioisomers (Figure 7). ¹H NMR (CD₂Cl₂): δ 3.9 (br s, CH₂CCH=C of isomer A), 2.9 (d, P(CH₃)₂Ph of isomer A, ²J_{P-H} = 13.1 Hz), 2.5 (d, PCH₃ of isomer B, ²J_{P-H} = 13.1 Hz), 2.4 (d, PCH₃ of isomer B, ²J_{P-H} = 13.1 Hz). ³¹P NMR (CD₂Cl₂): δ 27.4 (isomer B), 13.4 (isomer A). The relative intensities of the ¹H NMR doublets and the ³¹P NMR signals for this sample indicated a 32:68 ratio of isomer A to isomer B.

Syntheses of the Phosponium-1-indenylidene Ligands 1-C₉H₆PPh₃ (I), 1-C₉H₆PMePh₂ (II), and 1-C₉H₆PMe₂Ph (III). A mixture of 4.0 g of $[\text{1-C}_9\text{H}_7\text{PPh}_3]\text{Br}$ and 0.63 g of NaH (3-fold molar excess) in 60 mL of THF was stirred at room temperature for 48 h. The deep green solution was then filtered through Celite, and the solvent was removed under reduced pressure to give I as a dark green solid (2.58 g, 65% yield) which could be stored in air without decomposition. X-ray-quality crystals and analytically pure material were obtained by crystallization from a concentrated CH₂Cl₂ solution layered with hexanes. ¹H and ¹³C NMR data are given in Table 1, and the ¹H NMR spectrum is given in Figure S3 (Supporting Information). ³¹P NMR (CD₂Cl₂): δ 10.39. Anal. Found for C₂₇H₂₁P: C, 84.74; H, 5.50. Calcd: C, 86.10; H, 5.62.

The syntheses of 1-C₉H₆PMePh₂ (II) and 1-C₉H₆PMe₂Ph (III) were carried out similarly. Thus, a mixture of 7.85 g of $[\text{1-C}_9\text{H}_7\text{PMePh}_2]\text{Br}$ (19.9 mmol) and 0.53 g of NaH (22.0 mmol) in 150 mL of THF was stirred for 24 h at room temperature to yield 5.32 g of the pale green, air-sensitive II (85% yield). Pure material (NMR) could be obtained by crystallization from a concentrated CH₂Cl₂ solution layered with hexanes. A ¹H NMR spectrum is shown in Figure S4 (Supporting Information), while ¹H and ¹³C NMR data are given in Table 1; the data agree with literature values.⁴ ³¹P NMR (CD₂Cl₂): δ 5.69.

Similarly, a mixture of 2.39 g of $[\text{1-C}_9\text{H}_7\text{PMe}_2\text{Ph}]\text{Br}$ (7.2 mmol) and 0.19 g of NaH (7.9 mmol) in 60 mL of THF was stirred for 24 h at room temperature to yield, after solvent removal, 1.82 g of yellow-green, air-sensitive III (94% yield). A ¹H NMR spectrum is shown in Figure 3, while ¹H and ¹³C NMR data are given in Table 1. ³¹P NMR (CD₂Cl₂): δ 1.78. Anal. Found for C₁₇H₁₇P: C, 79.38; H, 6.69. Calcd: C, 80.93; H, 6.79. X-ray-quality crystals of I and III were obtained by

crystallization from a concentrated CH₂Cl₂ solution layered with hexanes.

Syntheses of $[\text{Ru}(\eta^5\text{-C}_5\text{H}_5)(\eta^5\text{-1-C}_9\text{H}_6\text{PPh}_3)]\text{PF}_6$ (IV), $[\text{Ru}(\eta^5\text{-C}_5\text{H}_5)(\eta^5\text{-1-C}_9\text{H}_6\text{PMePh}_2)]\text{PF}_6$ (V), and $[\text{Ru}(\eta^5\text{-C}_5\text{H}_5)(\eta^5\text{-1-C}_9\text{H}_6\text{PMe}_2\text{Ph})]\text{PF}_6$ (VI). In a typical reaction, a solution containing 0.13 g of $[\text{Ru}(\eta^5\text{-C}_5\text{H}_5)(\text{MeCN})_3]\text{PF}_6$ in 40 mL of CH₂Cl₂ and an equimolar amount of I, II, or III was stirred for 15 min. X-ray-quality crystals of IV–VI were obtained in all cases by the slow evaporation of saturated CH₂Cl₂ solutions, but bulk purification of the complexes was not readily accomplished. Compound IV was dissolved in a minimum amount of THF, and the solution was layered with hexanes or ethyl ether, but only impure product was obtained. Alternatively, IV was dissolved in a minimum amount of hot acetonitrile and the solution was cooled to –20 °C, but no precipitate formed. Similarly, compound V was dissolved in a minimum amount of THF or acetone and the solutions were layered with hexanes or toluene, respectively, but only impure product was obtained. Attempts to purify VI involved similar THF–hexanes, THF–ethyl ether, acetone–hexanes, and acetonitrile–ethyl ether layering experiments, but in all cases only impure product was obtained. Washing the impure products with benzene was found to remove some impurities, but judging from the elemental analyses and the ¹H NMR spectra, complete removal of all traces of solvent molecules was difficult. Elemental analysis confirmed that pure VI was obtained by washing with C₆H₆ followed by drying under vacuum for several days (Anal. Found: C, 46.79; H, 3.86. Calcd: C, 46.90; H, 3.94). This approach did not give analytically pure material for compounds IV (Anal. Found: C, 53.10; H, 4.04. Calcd: C, 55.90; H, 3.87) and V (Anal. Found: C, 49.48; H, 3.63. Calcd: C, 51.85; H, 3.81).

Computational Details. All geometry optimizations were carried out with Turbomole^{11,12} using the TZVP basis¹³ (small-core pseudopotential for Ru¹⁴) and the functional b3-lyp^{15–18} in combination with an external optimizer (PQS OPTIMIZE).^{19,20} Vibrational analyses were carried out for all stationary points to confirm their nature (0 imaginary frequencies). Final energies were obtained using the TZVPP basis,²¹ and these were combined with thermal corrections (enthalpy and entropy, 273 K, 1 bar) from the TZVP vibrational analyses to arrive at the final free energies. To account for the reduced freedom of movement in solution, entropy contributions to the free energies were scaled to two-thirds of their gas-phase values.^{22,23} Orbital plots in Figure 16 were made using Molden.²⁴ For a complete listing of energies, geometrical details, and final coordinate files, see the Supporting Information.

■ ASSOCIATED CONTENT

📄 Supporting Information

Text, figures, and tables giving the synthetic procedure for 1-bromoindene, NMR spectroscopic data for compounds I and III–VI and computational data and text, figures, tables, and CIF files giving crystallographic details for 1-C₉H₆PPh₃ (I), 1-C₉H₆PMe₂Ph (III), $[\text{Ru}(\eta^5\text{-C}_5\text{H}_5)(\eta^5\text{-1-C}_9\text{H}_6\text{PPh}_3)]\text{PF}_6$ (IV), $[\text{Ru}(\eta^5\text{-C}_5\text{H}_5)(\eta^5\text{-1-C}_9\text{H}_6\text{PMePh}_2)]\text{PF}_6$ (V), and $[\text{Ru}(\eta^5\text{-C}_5\text{H}_5)(\eta^5\text{-1-C}_9\text{H}_6\text{PMe}_2\text{Ph})]\text{PF}_6$ (VI), including complete numbering schemes, thermal ellipsoid figures, positional and thermal parameters, bond lengths, and bond angles. This material is available free of charge via the Internet at <http://pubs.acs.org>. The crystallographic data for 1-C₉H₆PPh₃ (CCDC 826560), C₉H₆PMe₂Ph (CCDC 826559), $[\text{Ru}(\eta^5\text{-C}_5\text{H}_5)(\eta^5\text{-1-C}_9\text{H}_6\text{PPh}_3)]\text{PF}_6$ (CCDC 826565), $[\text{Ru}(\eta^5\text{-C}_5\text{H}_5)(\eta^5\text{-1-C}_9\text{H}_6\text{PMePh}_2)]\text{PF}_6$ (CCDC 826564), and $[\text{Ru}(\eta^5\text{-C}_5\text{H}_5)(\eta^5\text{-1-C}_9\text{H}_6\text{PMe}_2\text{Ph})]\text{PF}_6$ (CCDC 826563) may also be obtained free of charge from The Cambridge Crystallographic Data Centre via www.ccdc.cam.ac.uk/data_request/cif.

ACKNOWLEDGMENTS

We thank the Natural Sciences and Engineering Research Council (Discovery Grants to M.C.B., P.H.M.B.) and Johnson-Matthey for a generous loan of RuCl₃·3H₂O.

REFERENCES

- (1) (a) Ramirez, F.; Levy, S. *J. Org. Chem.* **1956**, *21*, 488. (b) Ramirez, F.; Levy, S. *J. Org. Chem.* **1956**, *21*, 1333. (c) Ramirez, F.; Levy, S. *J. Am. Chem. Soc.* **1957**, *79*, 67. (d) Ramirez, F.; Dershowitz, S. *J. Org. Chem.* **1957**, *22*, 41. (e) Ramirez, F.; Levy, S. *J. Am. Chem. Soc.* **1957**, *79*, 6167. (f) Ramirez, F.; Levy, S. *J. Org. Chem.* **1958**, *23*, 2035. (g) Ammon, H. L.; Wheeler, G. L.; Watts, P. H. Jr. *J. Am. Chem. Soc.* **1973**, *95*, 6158. (h) Gray, G. A. *J. Am. Chem. Soc.* **1973**, *95*, 7736. (i) For a recent computational study, see: Laavanya, P.; Krishnamoorthy, B. S.; Panchanatheswaran, K.; Manoharan, M. *J. Mol. Struct. (THEOCHEM)* **2005**, *716*, 149.
- (2) For a comprehensive review of phosphonium cyclopentadienides and their coordination chemistry, see: Brownie, J. H.; Baird, M. C. *Coord. Chem. Rev.* **2008**, *252*, 1734.
- (3) (a) Brownie, J. H.; Baird, M. C.; Schmider, H. L. *Organometallics* **2007**, *26*, 1433. (b) Brownie, J. H.; Baird, M. C.; Laws, D. R.; Geiger, W. E. *Organometallics* **2007**, *26*, 5890.
- (4) Brownie, J. H.; Baird, M. C. *J. Organomet. Chem.* **2008**, *693*, 2812.
- (5) (a) Crofts, P. C.; Williamson, M. P. *J. Chem. Soc. C* **1967**, 1093. (b) Ford, J. A. *Tetrahedron Lett.* **1968**, 815.
- (6) Rufanov, K. A.; Ziemer, B.; Hummert, M.; Schutte, S. *Eur. J. Inorg. Chem.* **2004**, 4759.
- (7) Murphy, J. A.; Patterson, C. W. *J. Chem. Soc., Perkin Trans. 1* **1993**, 405.
- (8) Trost, B. M.; Older, C. M. *Organometallics* **2002**, *21*, 2544.
- (9) (a) Bart, J. C. J. *J. Chem. Soc. B* **1969**, 350. (b) Plíva, J.; Johns, J. W. C.; Goodman, L. *J. Mol. Spectrosc.* **1990**, *140*, 214.
- (10) (a) Cruickshank, D. W. J.; Sparks, R. A. *Proc. R. Soc. London, Ser. A* **1960**, *258*, 270. (b) Cadierno, V.; Díez, J.; Pilar Gamasa, M.; Gimeno, J.; Lastra, E. *Coord. Chem. Rev.* **1999**, *193–195*, 147.
- (11) Ahlrichs, R.; Bär, M.; Baron, H.-P.; Bauernschmitt, R.; Böcker, S.; Ehrig, M.; Eichkorn, K.; Elliott, S.; Furche, F.; Haase, F.; Häser, M.; Hättig, C.; Horn, H.; Huber, C.; Huniar, U.; Kattannek, M.; Köhn, A.; Kölmel, C.; Kollwitz, M.; May, K.; Ochsenfeld, C.; Ohm, H.; Schäfer, A.; Schneider, U.; Treutler, O.; Tsereteli, K.; Unterreiner, B.; Von Arnim, M.; Weigend, F.; Weis, P.; Weiss, H. *Turbomole Version 5; Theoretical Chemistry Group, University of Karlsruhe, Karlsruhe, Germany*, 2002.
- (12) Treutler, O.; Ahlrichs, R. *J. Chem. Phys.* **1995**, *102*, 346.
- (13) Schäfer, A.; Huber, C.; Ahlrichs, R. *J. Chem. Phys.* **1994**, *100*, 5829.
- (14) Andrae, D.; Häussermann, U.; Dolg, M.; Stoll, H.; Preuss, H. *Theor. Chim. Acta* **1990**, *77*, 123.
- (15) All Turbomole calculations were performed with the functional “b3-lyp” of that package, which is similar (but not identical) to the Gaussian “B3LYP” functional.
- (16) Lee, C.; Yang, W.; Parr, R. G. *Phys. Rev. B* **1988**, *37*, 785.
- (17) Becke, A. D. *J. Chem. Phys.* **1993**, *98*, 1372.
- (18) Becke, A. D. *J. Chem. Phys.* **1993**, *98*, 5648.
- (19) PQS version 2.4; Parallel Quantum Solutions, Fayetteville, AR, 2001 (the Baker optimizer is available separately from PQS upon request).
- (20) Baker, J. J. *Comput. Chem.* **1986**, *7*, 385.
- (21) Weigend, F.; Furche, F.; Ahlrichs, R. *J. Chem. Phys.* **2003**, *119*, 12753.
- (22) Tobisch, S.; Ziegler, T. *J. Am. Chem. Soc.* **2004**, *126*, 9059.
- (23) Raucoules, R.; De Bruin, T.; Raybaud, P.; Adamo, C. *Organometallics* **2009**, *28*, 5358.
- (24) Schaftenaar, G.; Noordik, J. H. *J. Comput.-Aided Mol. Design* **2000**, *14*, 123.